111-02-CR
211537
p54

THERMAL ANALYSIS OF A HYPERSONIC WING TEST STRUCTURE

NASA Grant NCC 2–433

Final Technical Report

October 1986 – April 1989

Prepared For

National Aeronautics and Space Administration

Ames Research Center

Dryden Flight Research Facility

Prepared By

Dr. Doral R. Sandlin
Principal Investigator

Neil J. Swanson, Jr.
Graduate Assistant

Aeronautical Engineering Department
California Polytechnic State University
San Luis Obispo, CA 93407

(NASA-CR-185319) THERMAL ANALYSIS OF A HYPERSONIC WING TEST STRUCTURE Final Report, Oct. 1986 - Apr. 1989 (California Polytechnic State Univ.) 54 p CSCL 01A N89-24265
Unclas
G3/02 0211537

Thermal Analysis of a Hypersonic Wing Test Structure with Comparison to Measured Data

Neil J. Swanson, Jr.
California Polytechnic State University
San Luis Obispo

Workshop on
Correlation of Hot Structures Test Data with Analysis

NASA Ames–Dryden Flight Research Facility
Edwards, California

November 15–17, 1988

Thermal Analysis of a Hypersonic Wing Test Structure with Comparison to Measured Data

- Selection of Regions for Analysis
- Description of Heat Transfer Mechanisms in the HWTS Wing Box
- Finite Element Methodology for Thermal Analysis of Hot Structures
- Comparisons of Calculated and Measured Structural Temperatures Distributions

ORIGINAL PAGE
BLACK AND WHITE PHOTOGRAPH

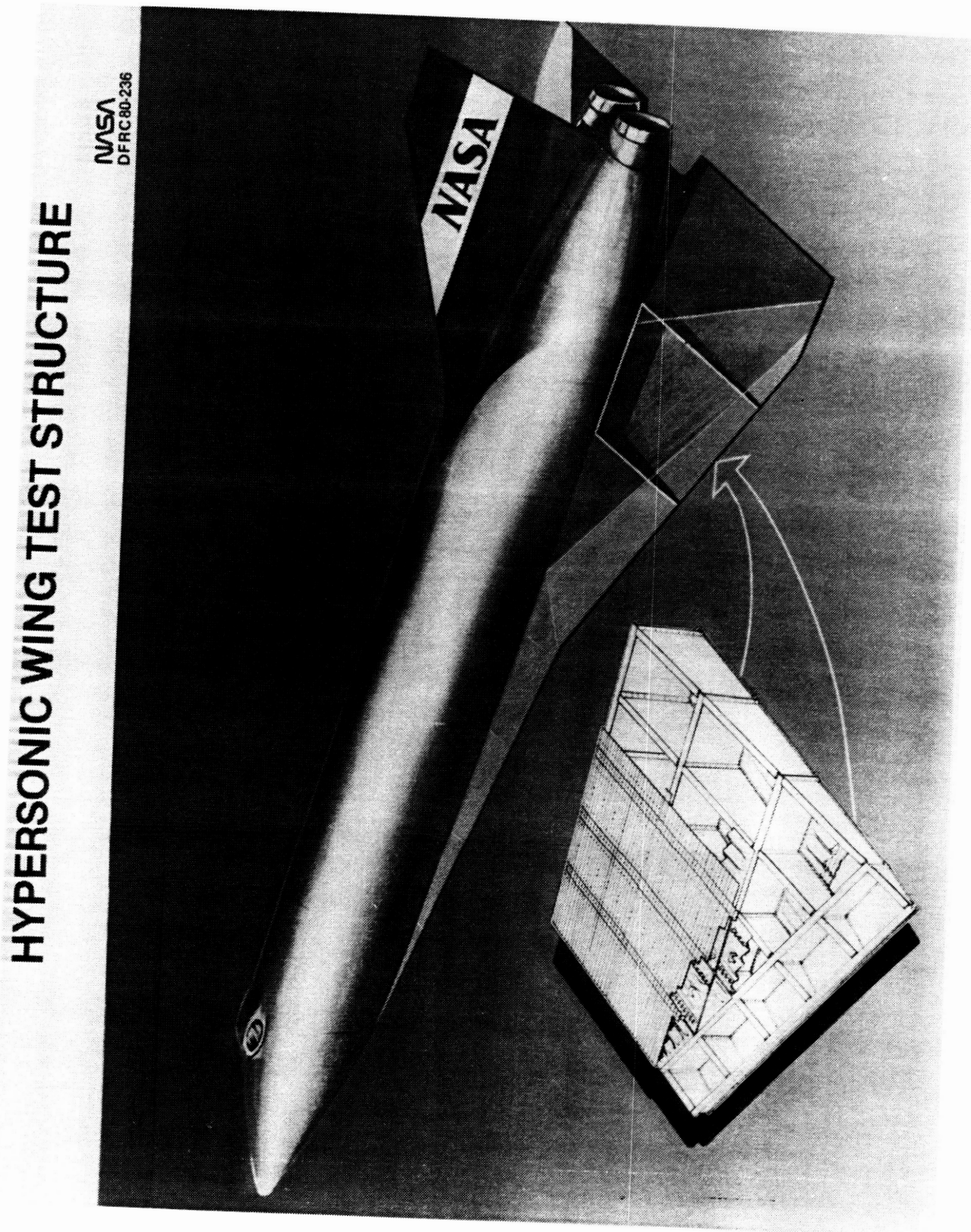

ORIGINAL PAGE
BLACK AND WHITE PHOTOGRAPH

Introduction
(Figure 1)

The National Aeronautics and Space Administration (NASA) has conducted elevated temperature structures research since the late 1940's [1]. In the 1950's and 1960's a large number of programs were directed at various vehicle/missions requiring flight at hypersonic speeds. Specifically, a number of promising structural concepts for application to a Mach 8 hypersonic research airplane were conceived at NASA Langley Research Center as part of a hypersonic aircraft study [2]. One of the earliest elevated structures studies for structures subjected to reentry heating can be found in Reference [3]. Subsequent studies [4] demonstrated the feasibility of hot load–carrying structures with radiative metallic thermal protection systems (TPS) for application to hypersonic airplanes. Additional investigations by Lockheed [5,6] of six metallic TPS hot wing structural concepts selected the spanwise–stiffened beaded semimonocoque wing–box panel as the best concept based on least total system cost. As part of a hot structures research program at the NASA Ames–Dryden Flight Loads Research Facility (FLRF) [7] this concept has undergone subsequent development [8], including design optimization and concept verification testing at both the elemental [9] and component levels [10].

Shuttle experience has demonstrated a number of analytical technology needs for the design of future aerospace vehicles subjected to reentry heating. The thermal analysis of the shuttle wing during reentry illustrates the limitations, capabilities, and flexibility of the existing thermal and structural analysis methods. The shuttle wing thermal analysis consists of 118 three–dimensional, lumped parameter finite difference local models each having about 200 nodes. Temperature are computed in each local model and then interpolation is used between models to obtain temperatures in the unmodeled regions. This method is tedious, laborious, and time–consuming and has lead to underpredicted (unconservative) thermal stresses [11].

Consequently, three NASA centers (Ames–Dryden, Johnson, and Langley) have undertaken a coordinated effort to develop improved thermostructural analysis techniques. These improvements will include : 1) methods to automate the more tedious aspects of generating lumped–parameter and finite element thermal models; 2) faster solution techniques for large–order matrix equations governing nonlinear, transient heat transfer; 3) methods to transfer temperatures from a thermal finite element model to a dissimilar structural finite

element model; 4) methods of automating the determination of the times at which the critical combinations of thermal and mechanical internal loads occur; and 5) improved modeling procedures to reduce model size. This effort will also include the verification of procedures through comparison with experimental results obtained from large representative structural components.

The present report[1] is part of the effort to develop improved thermostructural analysis techniques. Specifically, this report describes the three–dimensional finite element modeling techniques developed for the thermal analysis of a hypersonic wing test structure (HWTS) which has been extensively tested at the FLRF. The computed results are compared to measured test data. In addition, the results of a NASA two–dimensional lumped parameter finite difference local thermal model [12] and the results of a contractor's two–dimensional lumped parameter finite difference local thermal model [13] will be presented.

[1] The NASA Technical Officer for this grant is Mr. Leslie Gong, NASA Ames–Dryden Flight Research Facility, Edwards, California.

ORIGINAL PAGE
BLACK AND WHITE PHOTOGRAPH

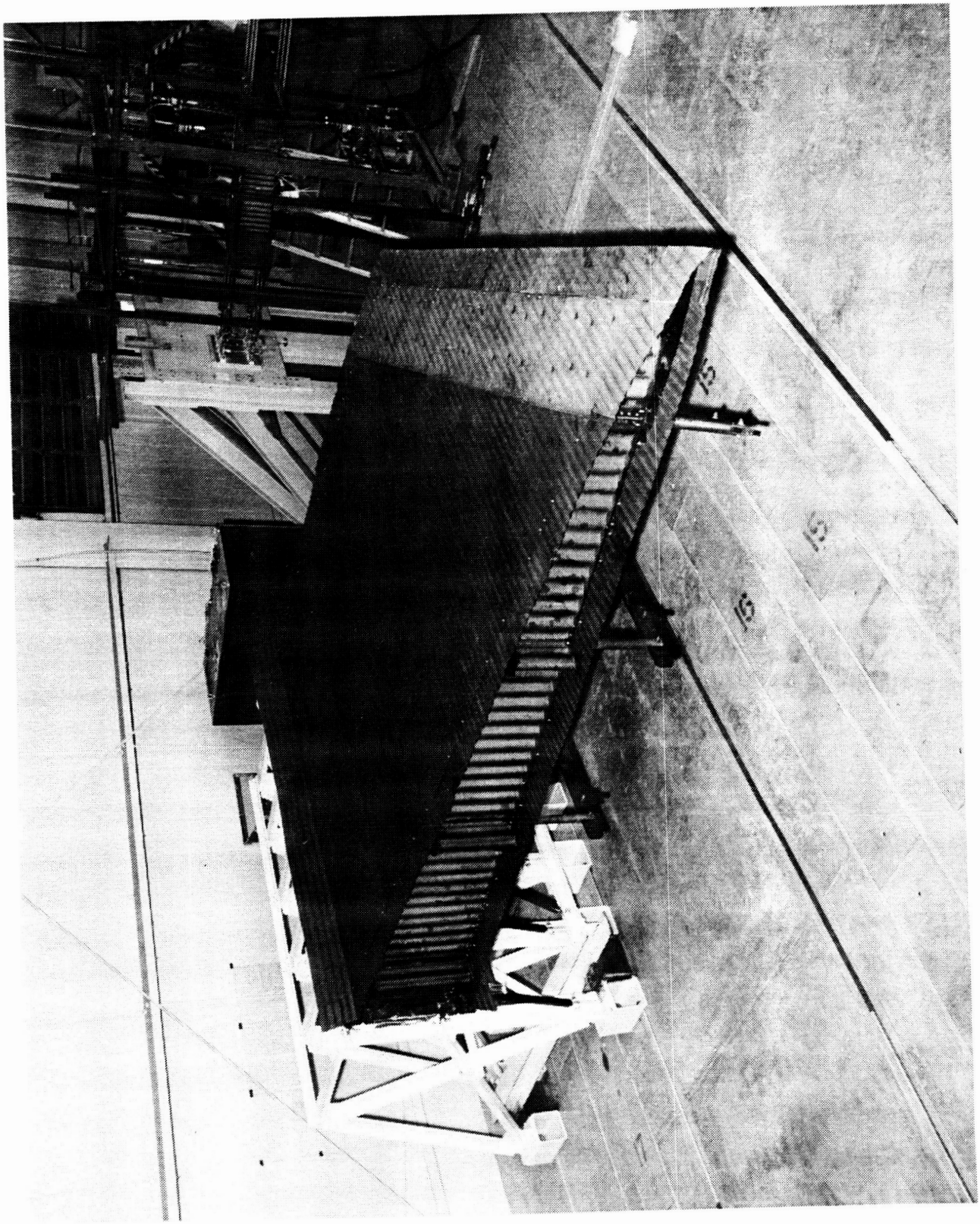

Wing Locations Analyzed
(Figure 2)

The configuration of the Hypersonic Research Airplane (HRA) concept is shown in figure 2, is a single–place design with horizontal takeoff and landing capability. The airplane, designed for Mach 8 flight, is 101 ft long, has a wing span of 38 ft and is a discrete wing–body with a single vertical tail. It has an estimated gross weight of 72 582 lb.

The wing and vertical tail are hot, radiating–type structure fabricated primarily from superalloys. The starboard wing shows the general dimensions and shape of the HWTS with a transition section. The crosshatched area shows the location of the inboard center wing bay which was the area selected for thermal analysis. This area was selected because it is the most heavily instrumented.

Wing Locations Analyzed

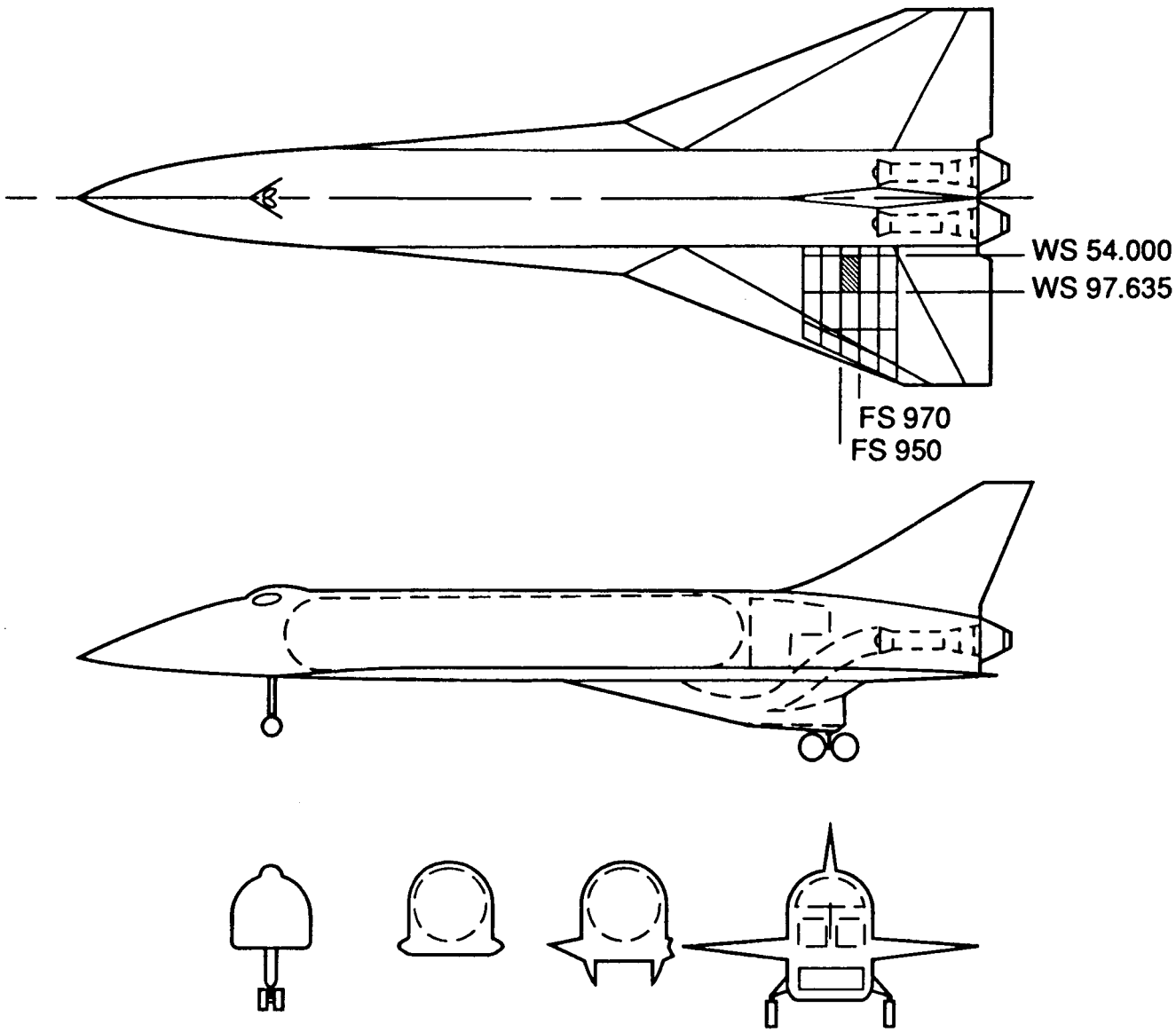

HWTS Loads Environment for Mach 8 Cruise
(Figure 3)

Figure 3 is a time history of the loads environment experienced by the HRA for a Mach 8 cruise at approximately 100 000 ft. A major design consideration was the pushover–pullup loads maneuver shown in figure 3. This maneuver requires a 3–minute transition maneuver performed from the initial cruise condition to the initial loads maneuver condition. This transition maneuver is performed in such a way that it is not a design condition, and the aircraft has obtained radiation equilibrium temperatures before performing the loads maneuver. The loads maneuver is initiated at Mach 8 at an altitude of 90 000 ft, and consists of a –0.5 g pushover, a 2.5 g pullup, and a return to the nominal research mission descent profile.

HWTS Loads Environment for Mach 8 Cruise

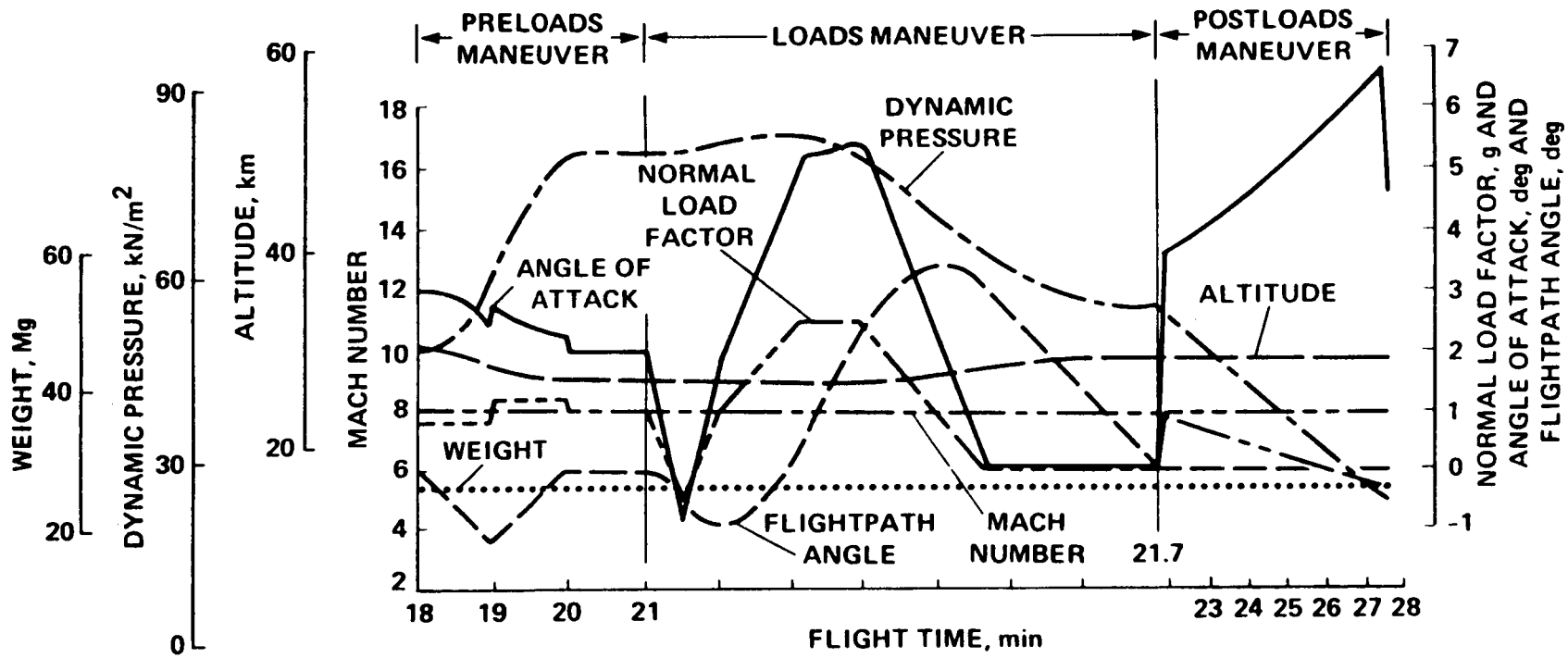

Typical HWTS Structure
(Figure 4)

A cord–wise cross section of the inboard center wing bay of the HWTS is shown in this figure. The basic construction consists of slightly corrugated non–load bearing stand–off heat shields connected to Z–clips which are in turn connected to channels. The channels are spot welded to beaded structural panels. The structural panels are connected to corrugated spar and rib webs. In addition, pressure pans are installed in all inboard wing bays so that pressure forces may be applied normal to lower inboard structural panels. The center wing bay components are fabricated of René 41 with the exception of the pressure pans, which are manufactured of stainless steel 321.

The heat transfer problem statement is as follows: the boundary conditions consist of specified temperature–time distributions on both the upper and lower heat shields, insulated or zero heat flow boundary conditions on the outer surfaces of the rib and spar webs, all other surfaces may exchange radiation with each other. Internal conditions such as contact resistance were not considered because conduction in these thin gauge structures is a least an order of magnitude smaller than radiation. Free convection within the wing box was not considered because the wing was tested inverted for structural reasons, the windward or hotter surfaces nearer the sky and the leeward or cooler surfaces near the ground in the test setup. At approximately 800 seconds into the heating profile 5 psig nitrogen is introduced into the pressure pans .

Typical HWTS Structure

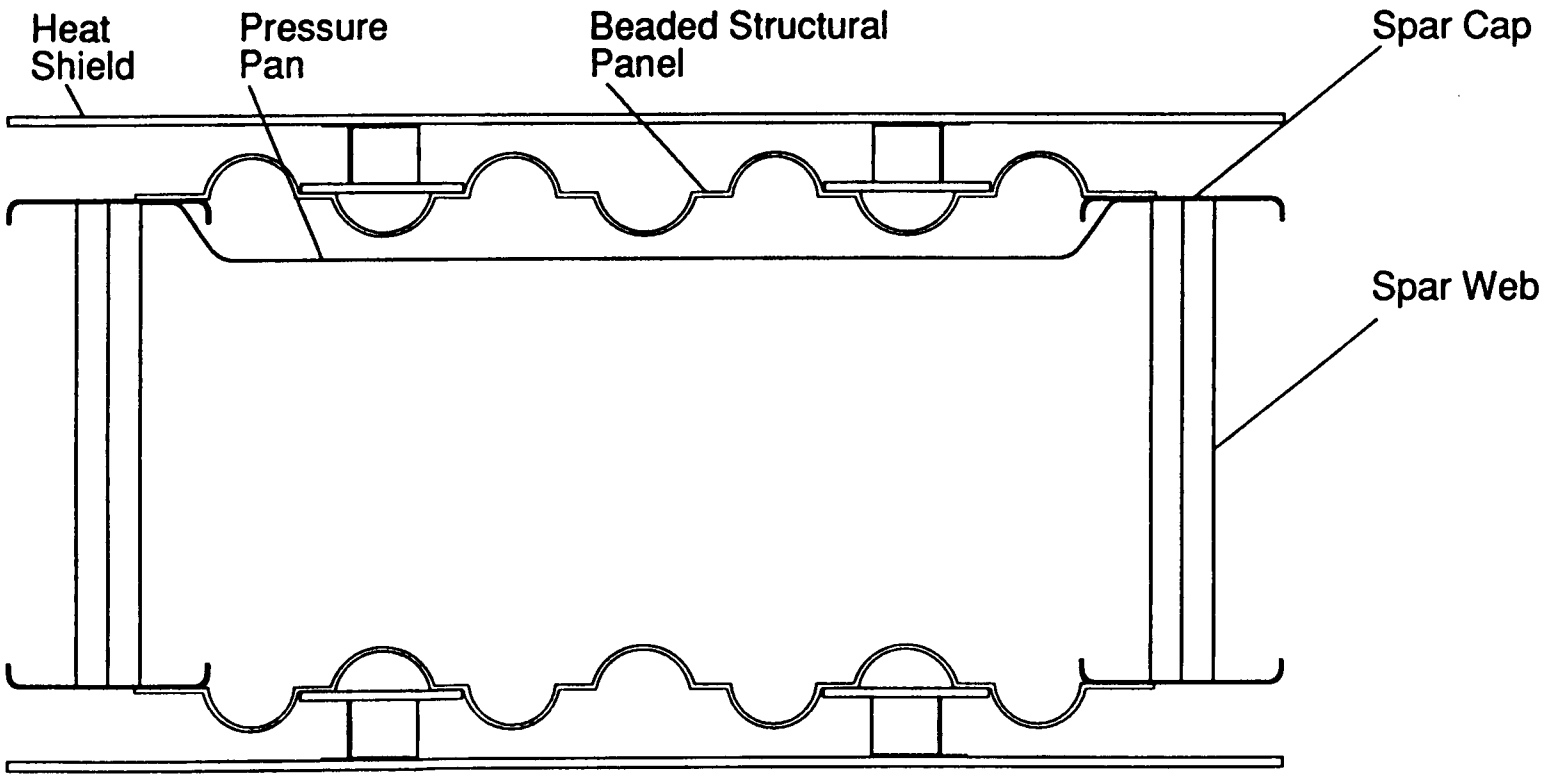

Hypersonic Wing Test Structure with Heat Shields Removed
(Figure 5)

Figure 5 shows the HWTS mounted in a support fixture with the heat shields removed. Z–shaped clips are used to connect the heat shields to the structure. The HWTS has six spars perpendicular to the aircraft centerline, producing five chord–wise bays. The outboard portion of the structure between the leading edge rib and the 30% rib is covered by an insulation packet; the insulation is intended to keep maximum structural temperatures below 1800 °F and to keep spanwise temperature gradients constant.

ORIGINAL PAGE
BLACK AND WHITE PHOTOGRAPH

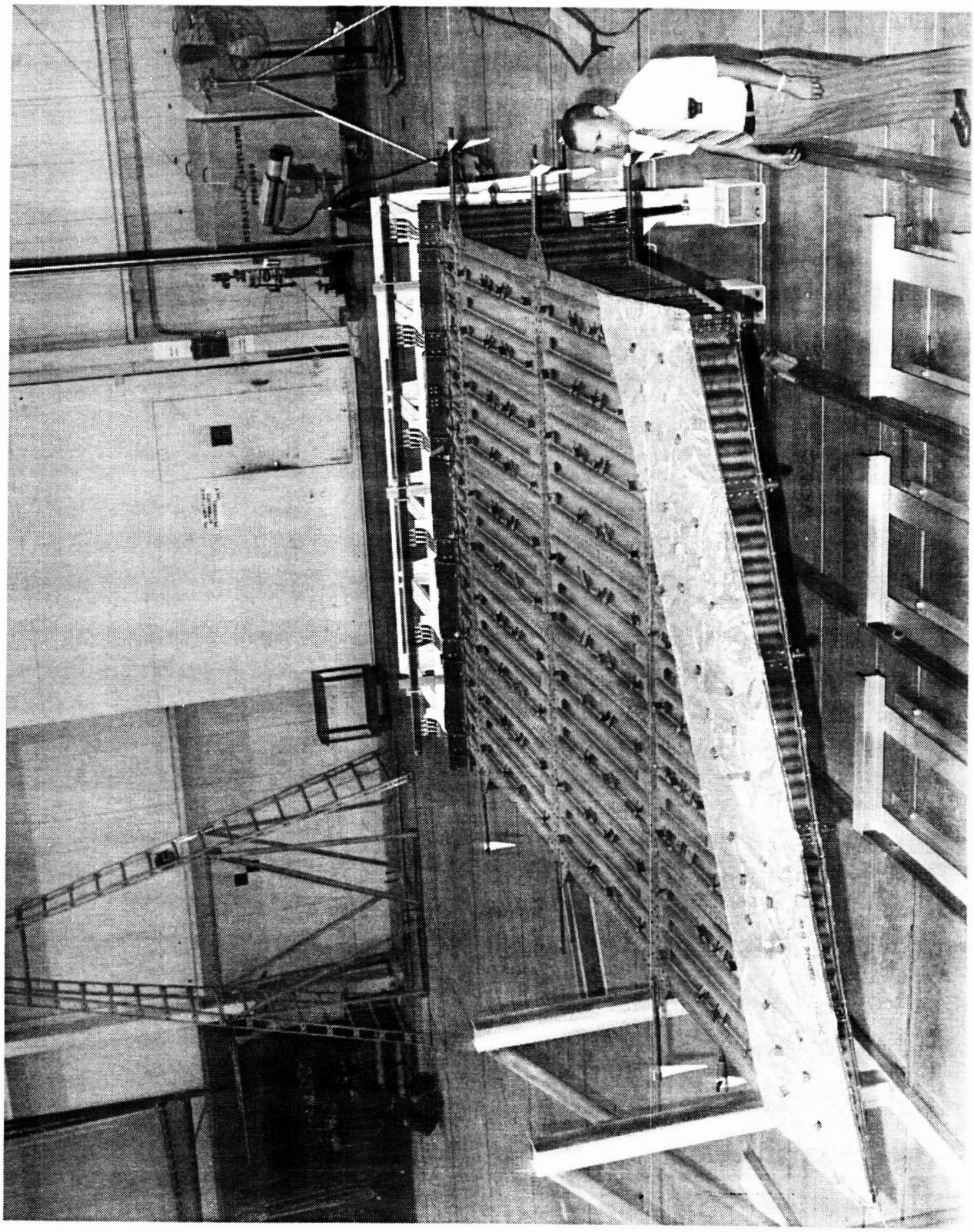

Interior of Hypersonic Wing Test Structure with and with Pressure Pans
(Figure 6)

Figure 6 (a) shows the interior of the HWTS without pressure pans. To apply pressure loads normal to the beaded panel surfaces, pressure pans were constructed and added to the HWTS. Figure 6 (b) shows the top view of a pressure pan exposed by removing an upper beaded panel. Two lines are attached to the pan; the larger one is a pressure feedline and the other is a pressure monitor line. Each lower surface root panels is backed by a pressure pan so an internal pressure of 5 psig can be applied to the panels during testing.

ORIGINAL PAGE
BLACK AND WHITE PHOTOGRAPH

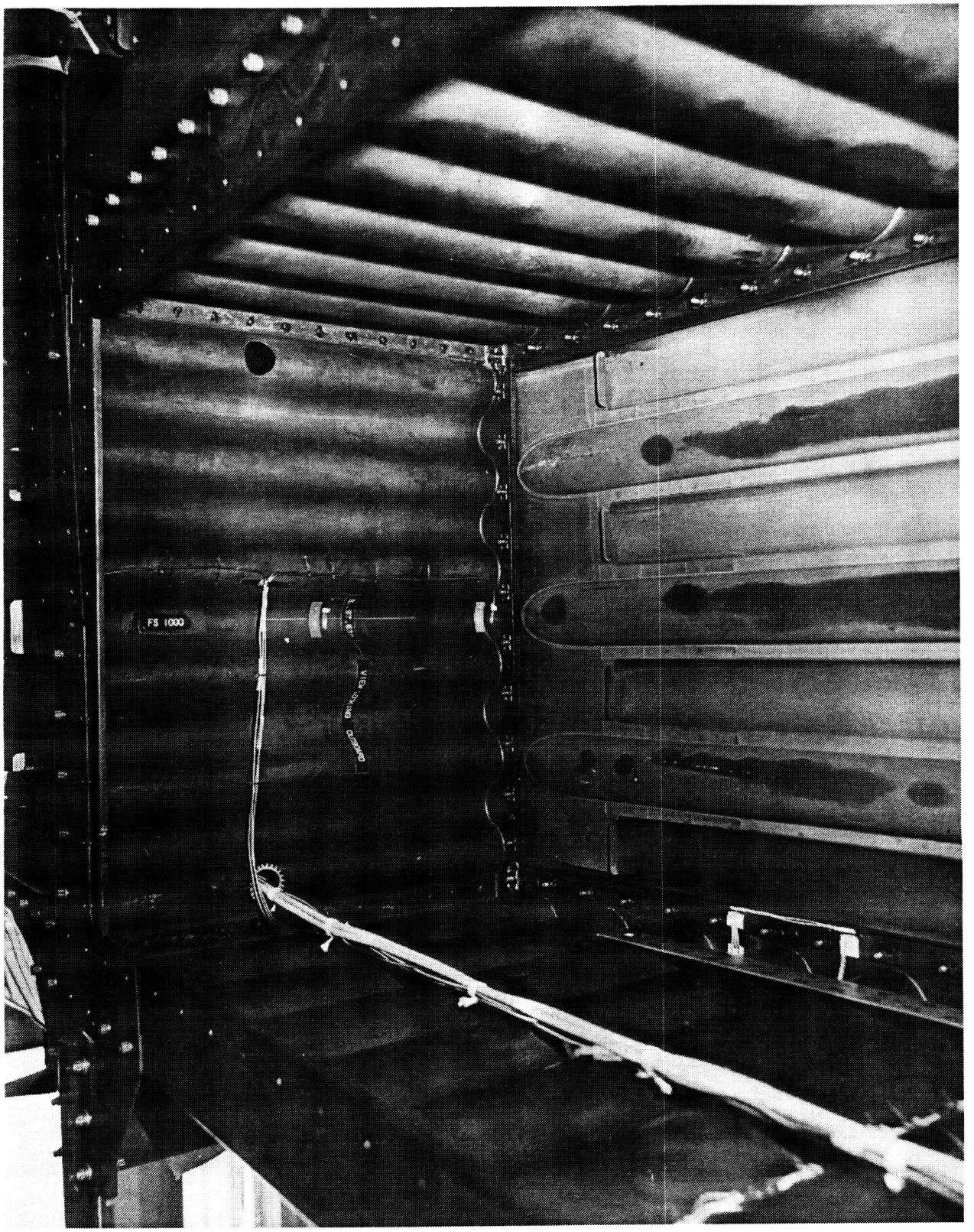

ORIGINAL PAGE
BLACK AND WHITE PHOTOGRAPH

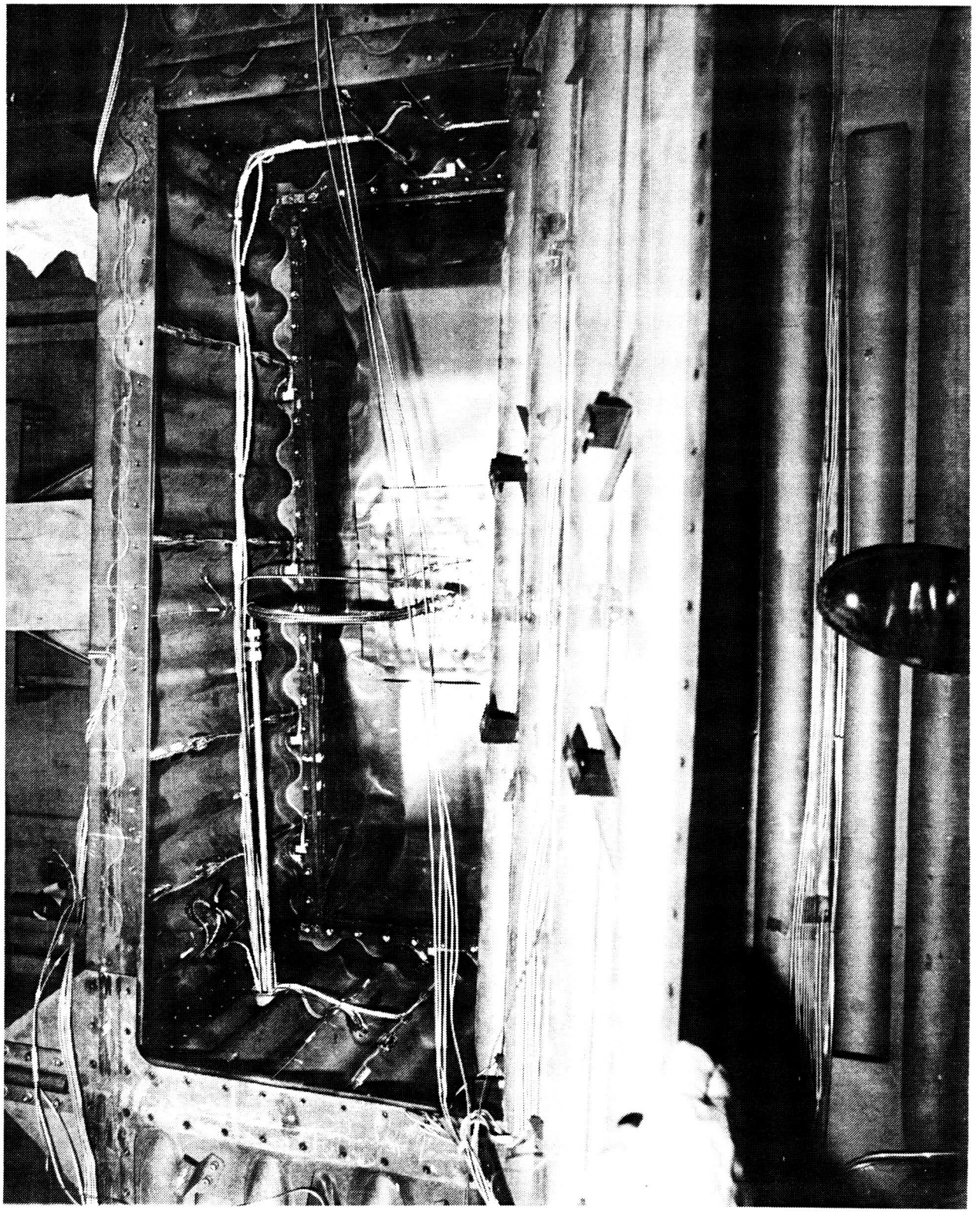

Thermocouple Locations
(Figure 7)

A total of 296 thermocouples were installed on the HWTS as shown in figure 7. One hundred thirty–one were located on spars and ribs, 76 on beaded skin panels, and 89 on the heat shields.

Thermocouple Locations

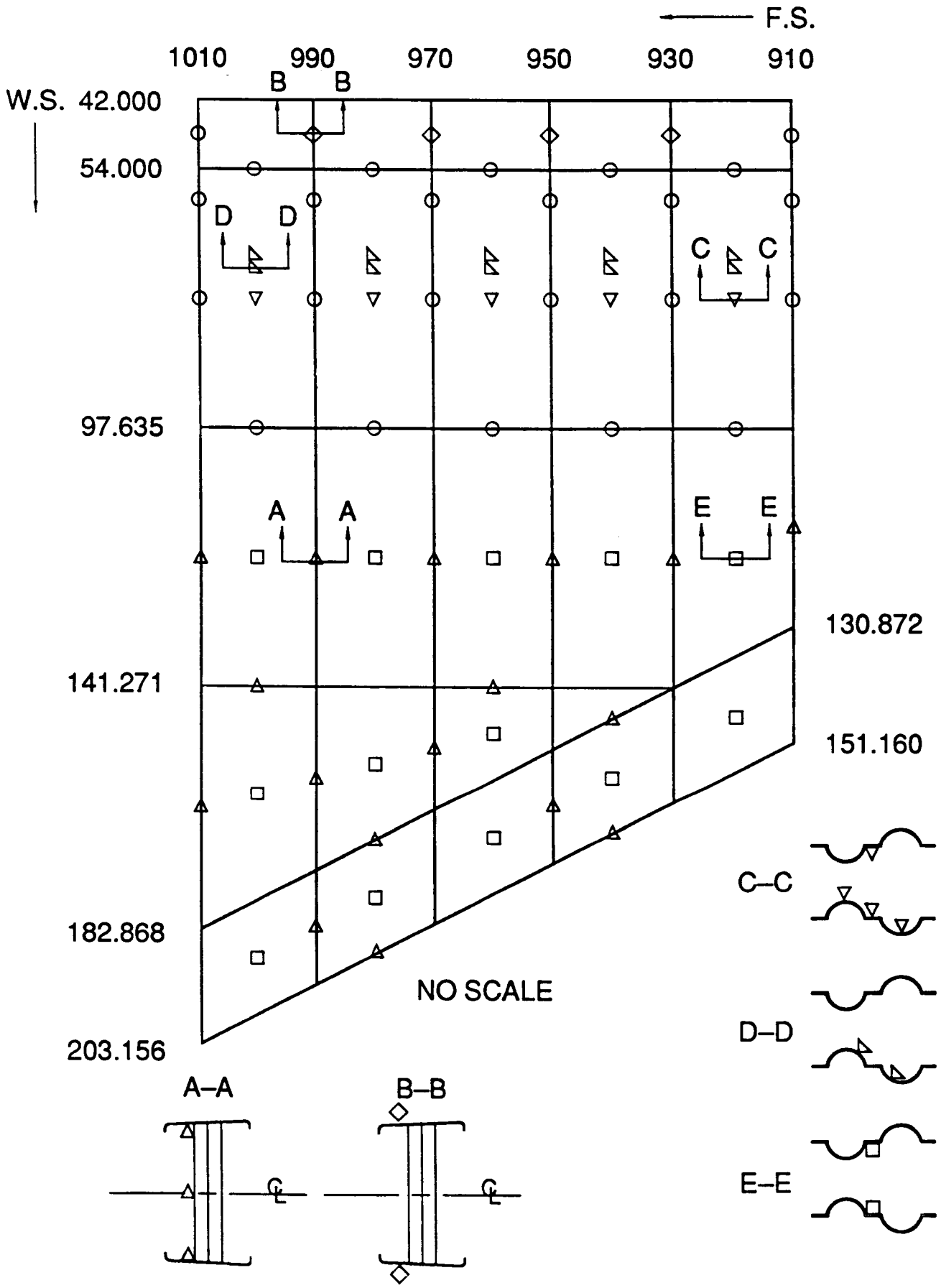

Measured Bead Temperatures for Lower Structural Panel
(Figure 8)

This figure shows the measured temperature difference between upward and downward facing beads on a lower structural panel. Point A is located on a upward facing bead (closest to lower heat shield) and point B is located on a downward facing bead. Point A is hotter than B because point A has a unobstructed view of lower heat shield. The solid line shows that a maximum temperature difference of 100 °F between upward and downward facing beads occurs at approximately 800 seconds. As the HWTS approaches radiation equilibrium temperatures during the later times in the heating profile, this temperature difference decreases to approximately 10 °F. This figure provides a measure of the level of uncertainty involved when comparing measured transient temperatures with predicted transient temperatures (since all thermal modeling of the HWTS have used thermal elements which are not corrugated, but are planar of uniform equivalent thickness).

Measured Bead Temperatures for Lower Structural Panel

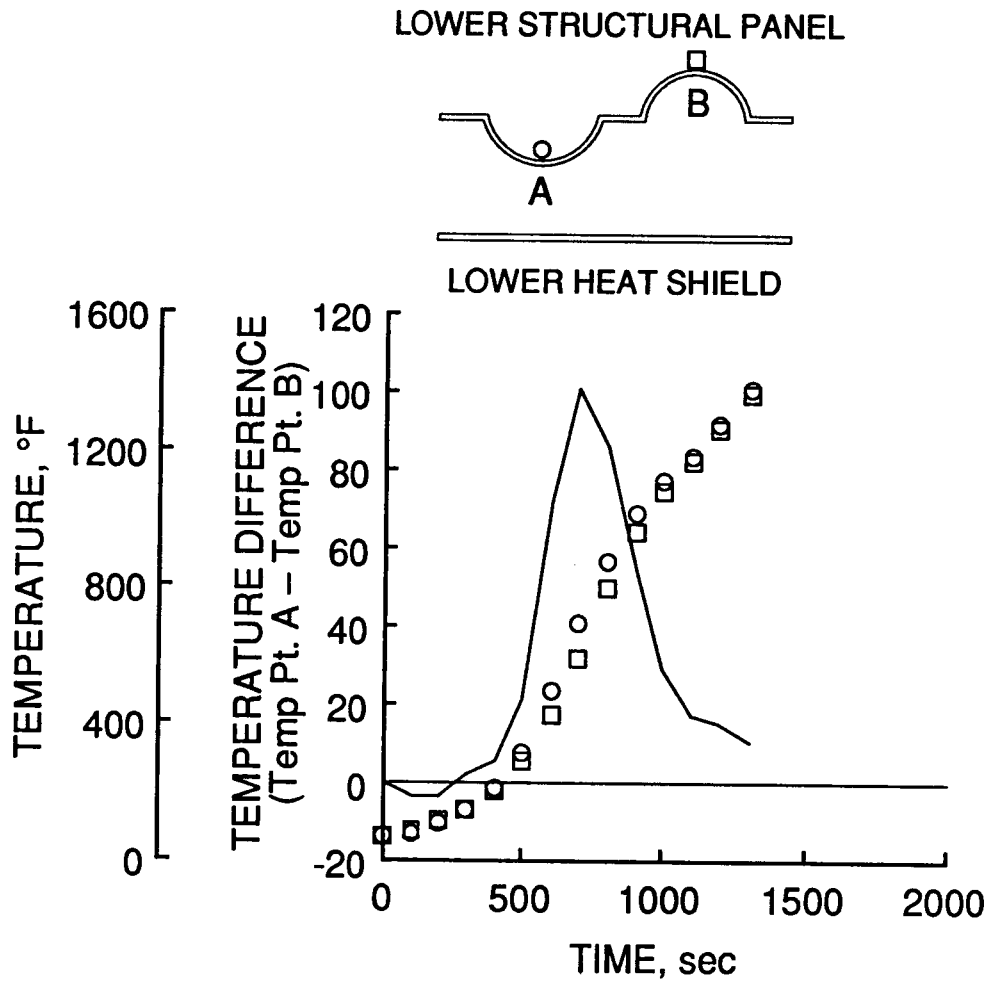

Thermal Effects of Corrugations
(Figure 9)

Radiation

When radiation enter a corrugated surface, the ensuing reflections and re–reflections among the corrugations provide additional opportunities for energy absorption. Thus the energy absorbed within a corrugated surface will generally exceed that which would be absorbed by a plane surface of identical absorptance. Similarly, the multiple reflections within a corrugated surface act to augment the emissive power of the corrugated surface relative to that of a plane surface of identical temperature and emittance. Consequently, the thermal effect of corrugations is to cause a increased effective emittance and absorptivity as compared to a plane surfaces.

Conduction

The conduction path measured along the corrugations is greater than the conduction path of a plane surface of the equal projected area and equivalent uniform thickness. Consequently, for the modeling of corrugated surfaces as plane surfaces it is necessary to reduce the thermal conductivity of the plane surface in the direction of the corrugations.

Thermal Effects of Corrugations

Thermal Effect	Modeling Methodology
Radiation	
Increased effective emittance as compared to planar surface	Model as planar elements of increased emittance
Conduction	
Increased conduction path along corrugations	Model as planar elements with reduced longitudinal thermal conductivity

Corrugated Element

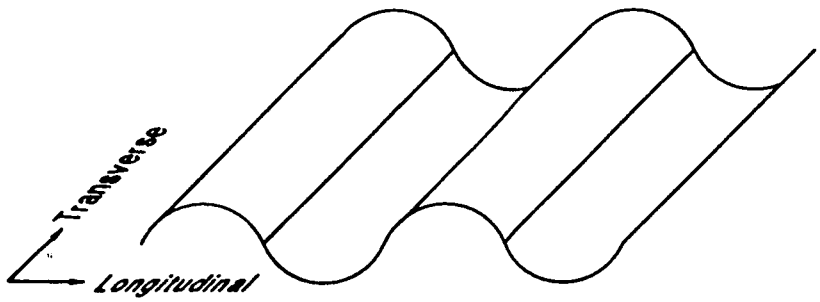

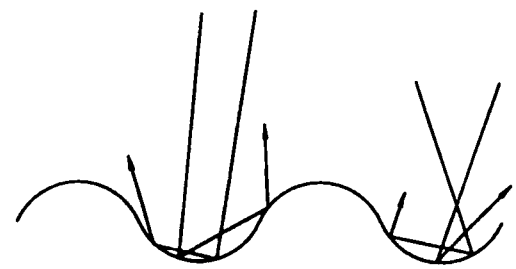

Planar Element

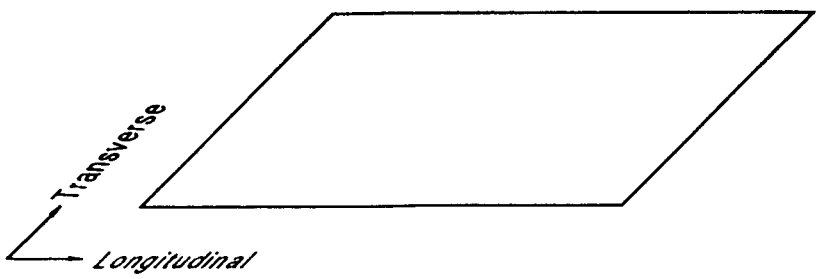

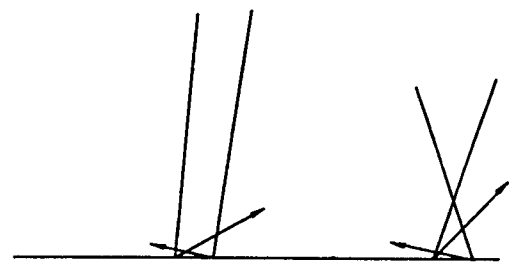

Design Two Dimensional Finite Difference Thermal Model of the HWTS Wing Box (Figure 10)

Figure 10 shows the nodalization utilized for the design two dimensional finite difference thermal model of the HWTS wing box. A typical model consists of 10 nodes. Radiant heat interchange occurs between elements 1 and 2, all elements 2 through 9, and 9 and 10. Conductive heat interchange between elements 5 and 6 were determined to have little effect on final temperatures so this heat path was deleted by the contractor.

Design Two Dimensional Finite Difference Thermal Model of HWTS Wing Box

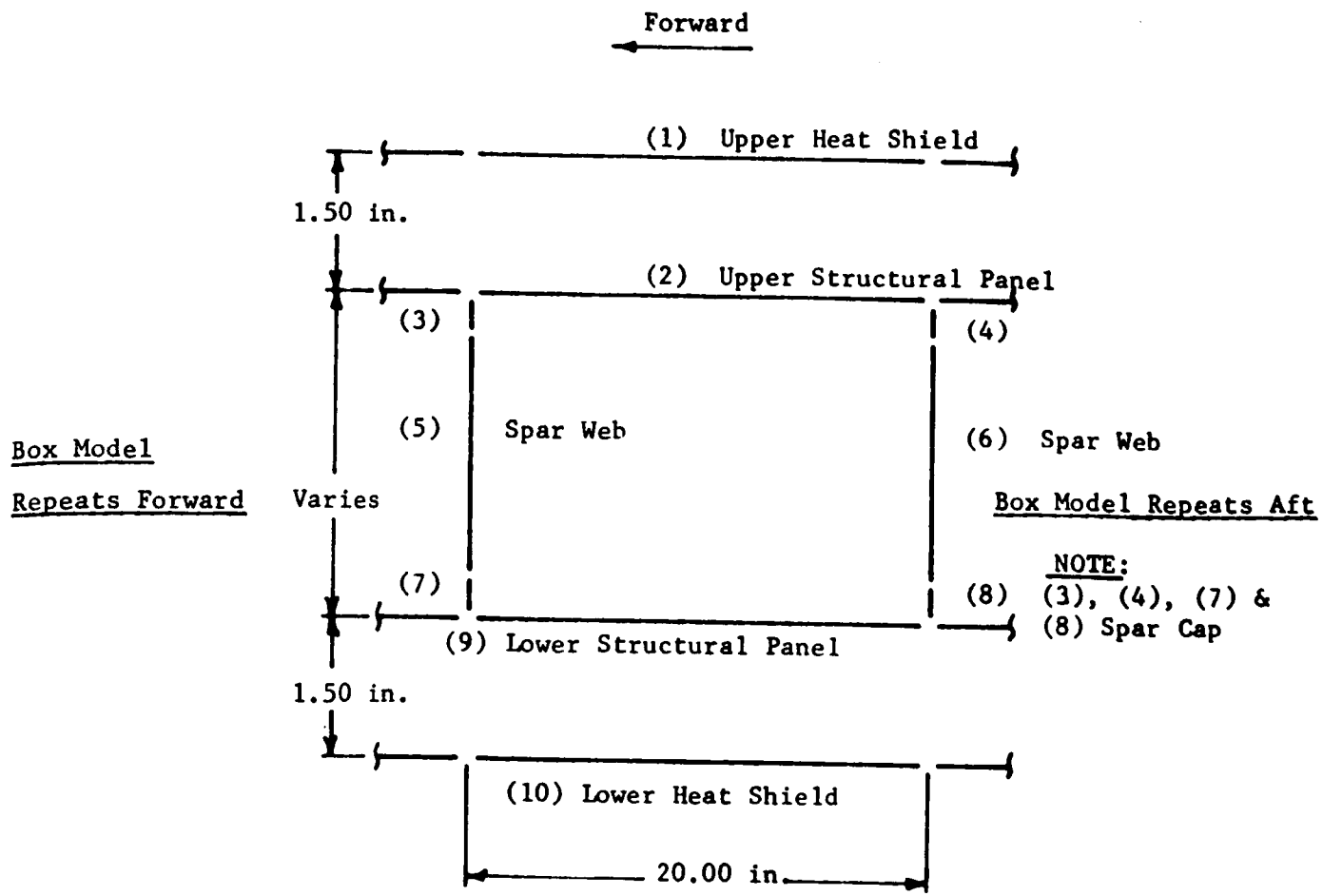

Comparison of Measured and Design Calculated HWTS Fuselage Temperatures (Figure 11)

A comparison of selected design temperature histories with measured data is shown in figure 11. Agreement between the measured and design temperatures is in general poor. However, it may be noted that the largest discrepancies occur during the high heating part of the profile and agreement improves near the end of the profile. It should be noted here that the pressure pans were not included in the design thermal models.

The trend illustrated in this figure between predicted and measured data is typical of all the thermal modeling performed on the HWTS, predicted temperatures tend to overpredict measure data during the periods of highest heating and improve somewhat as the structure approaches its radiation equilibrium temperature.

Comparison of Measured and DESIGN Calculated HWTS Fuselage Temperatures

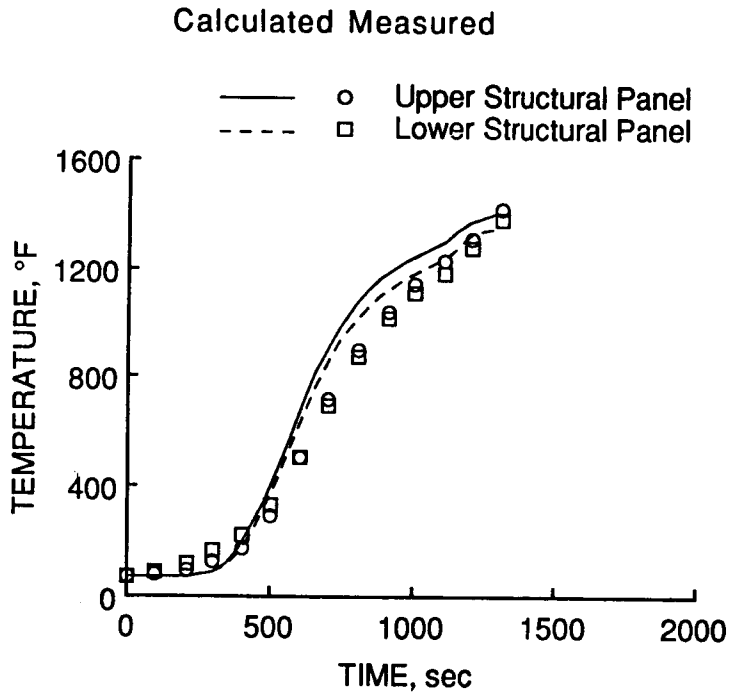

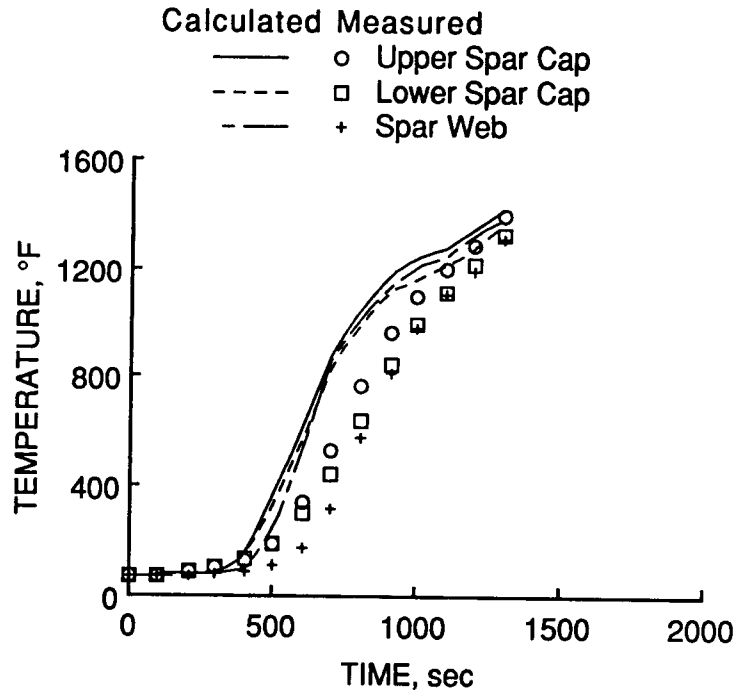

NASA Two Dimensional Finite Difference Thermal Model of HWTS Wing Box (Figure 12)

Figure 12 shows the nodalization utilized for the NASA two dimensional finite difference thermal model of the HWTS wing box. There are a total of 26 capacitors, 22 conduction resistors, and 100 radiation resistors. The spar web is divided into 9 nodes through its depth and the structural panels are divided into 5 nodes.

NASA Two Dimensional Finite Difference Thermal Model of HWTS Wing Box

LTA Thermal Model	Capacitors	Resistors	
		Conduction	Radiation
HWTS54	26	22	100

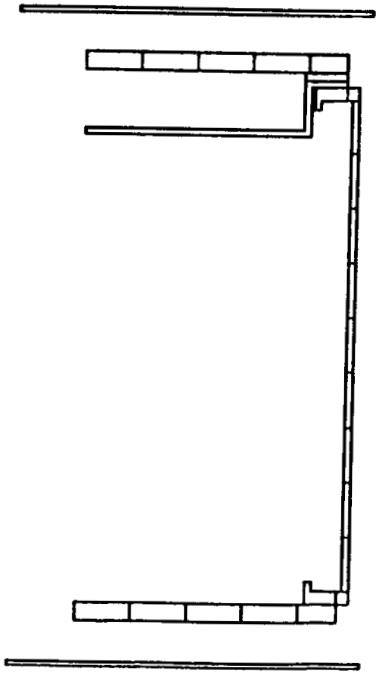

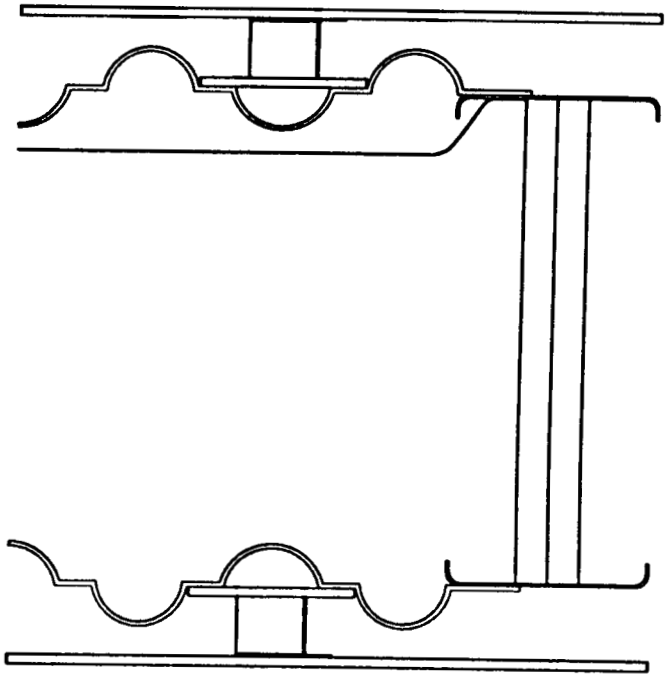

Comparison of Measured and NASA Calculated HWTS Fuselage Temperatures (Figure 13)

Temperatures of the upper and lower structural panels and the spar webs are shown in figure 13. The measured and calculated data of the structural panels are in good agreement during the first 800 sec of the profile. After 800 sec, calculations tend to overpredict the measured data with a maximum difference of 54 °F occurring at 1 000 sec on the upper structural panel. Spar temperatures are in good agreement during the first 600 sec of the profile. After 600 seconds, the calculated spar cap temperatures are approximately 54 °F higher than the measured data. The calculated web temperatures show a marked departure from the measured values after 800 sec and overpredict the measured data by as much as 117 °F at 1 000 sec.

Comparison of Measured and NASA Calculated HWTS Fuselage Temperatures

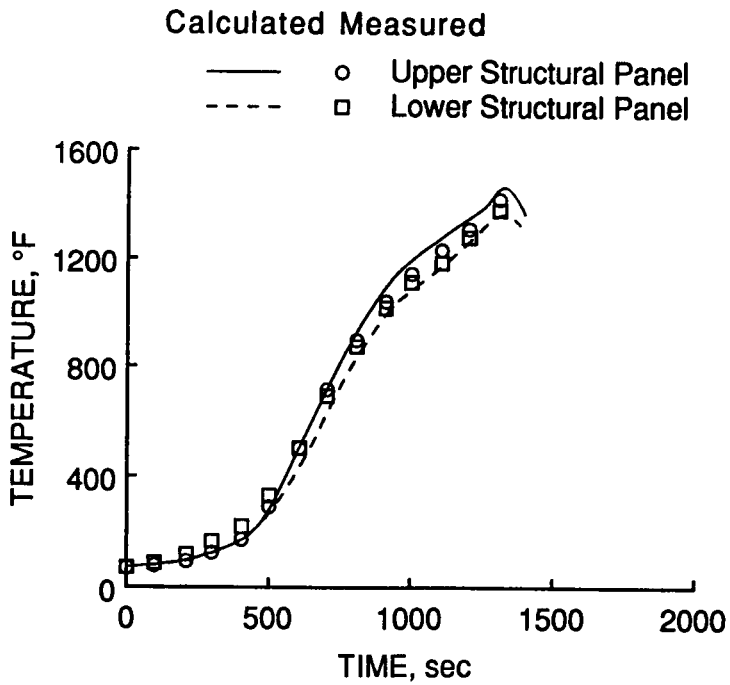

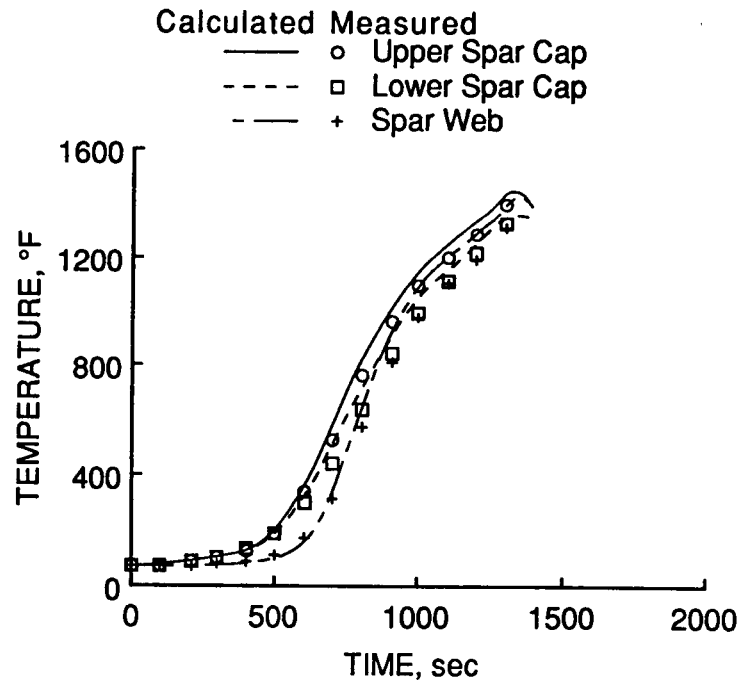

Three Dimensional SPAR Thermal Model of the HWTS Wing Box (Figure 14)

The finite-element model, figure 14, was constructed using the finite-element program Structural Performance And Resizing (SPAR). The structural panels, spar webs, spar caps, rib webs, and rib caps were modeled with K41 elements (four-node heat conduction elements). The internal radiation and the radiation from the heat shields to the structural panels were modeled by attaching R41 (four-node radiation elements) to the radiating surfaces.

Because of the complex nature of the HWTS a number of simplifing assumptions were made so that the analysis would be more tractable using existing computers. Firstly, all structural elements (rib webs, spar webs, etc.) were modeled as thermally thin plates (or lumps) of uniform equivalent thickness. This actual wing structure is corrugated and the modeling structural elements as flat plates of uniform equivalent thickness is valid because (1) for a thin skinned structure at very high temperatures, radiation heat transfer within a structure is usually at least an order of magnitude greater than conduction heat transfer, and (2) the effective emittance increase caused by the corrugations is small and need not be considered. Secondly, all internal radiation was assumed to originate from gray diffusely reflecting surfaces of constant emittance. (Diffuse surfaces emit and reflect radiation uniformly in all directions; gray surfaces emit energy independent of wave length.) This assumption may not be valid, however, the considerable reduction in mathematical complexity of a diffuse-gray analysis makes this assumption reasonable as a first approximation. Reflected radiation was accounted for by using the radiosity method of Eckert and Drake.

Three Dimensional SPAR Thermal Model of HWTS Wing Box

SPAR Thermal Model	JLOCS	Element		Fij
		K41	R41	
SHWTS4	110	130	172	8426

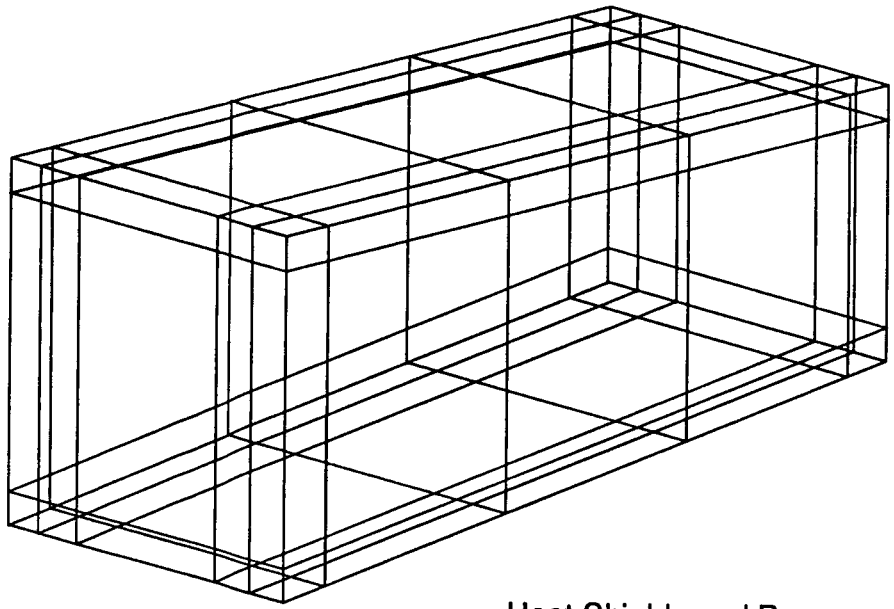

Heat Shields and Pressure Pan Not Shown

Comparison of Measured and Calculated HWTS Fuselage Temperatures (Figure 15)

Temperatures of the upper and lower structural panels are shown in the top right of figure 15. Again, the measured and calculated data of the structural panels are in good agreement during the first 800 seconds of the profile, after which the calculations tend to overpredict the measured data. Spar temperatures are shown in the lower right and left of figure 15 and are in good agreement during the first 600 seconds of the profile. After 600 seconds, the calculated spar cap temperatures also tend to overpredict measured data. The greatest discrepancies between measured and calculated temperatures occurs on the spar webs after 800 seconds. Again note that the agreement between measured and calculated temperatures improve somewhat as the structure approaches its radiation equilibrium temperature.

Comparison of Measured and Calculated HWTS Fuselage Temperatures

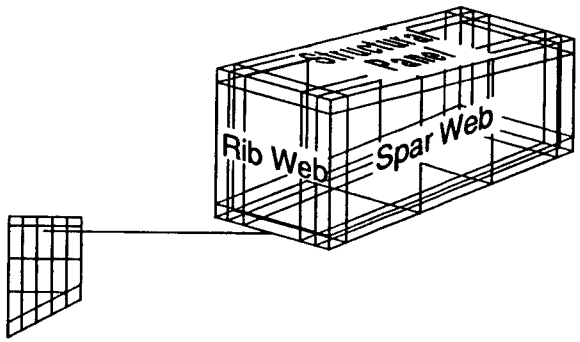

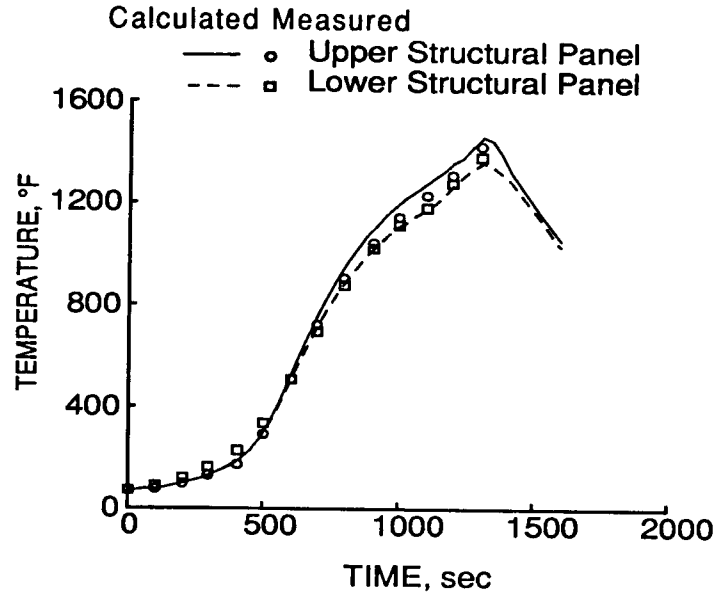

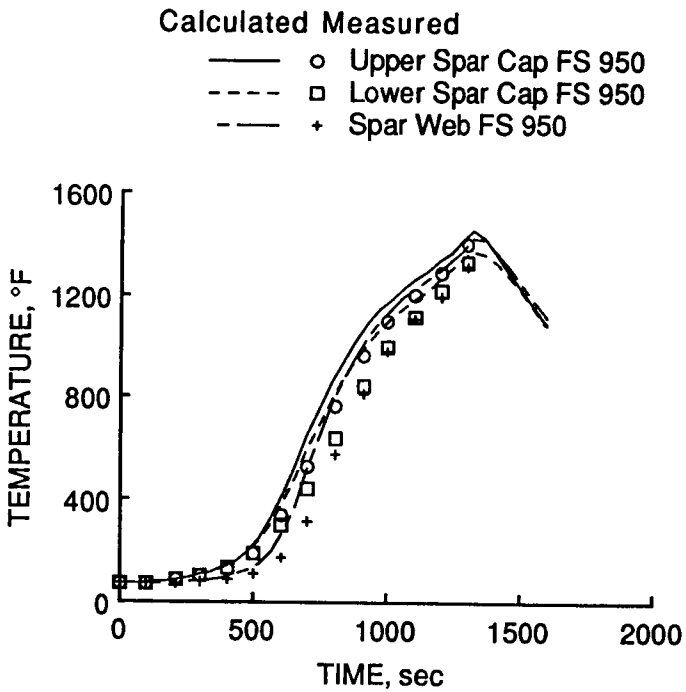

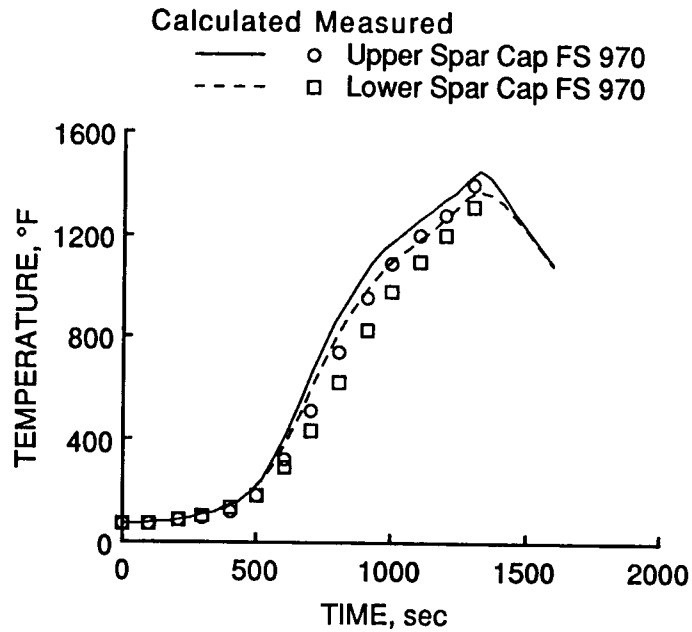

Comparison of Measured and Calculated HWTS Fuselage Temperatures (Figure 16)

Temperatures of the of the rib caps and webs are shown in figure 16. The greatest discrepancies between measured and calculated temperatures occurs on the inboard rib cap and webs after 500 seconds. Such a large discrepancy indicates an overall heat loss from the system. This suggest that the insulated or zero heat flow boundary conditions on the outer surfaces of the rib and spar webs are not correct. Immediately inboard of the bay selected for analysis is a transition section. Although not part of the aircraft design, the transition section was included to provide a buffer between the support structure and the test portion of the wing. It is likely that a spanwise heat flow exists from the hotter leading edge areas to the cooler inboard transition and support structure areas which would account for the heat loss from the system.

Comparison of Measured and Calculated HWTS Fuselage Temperatures

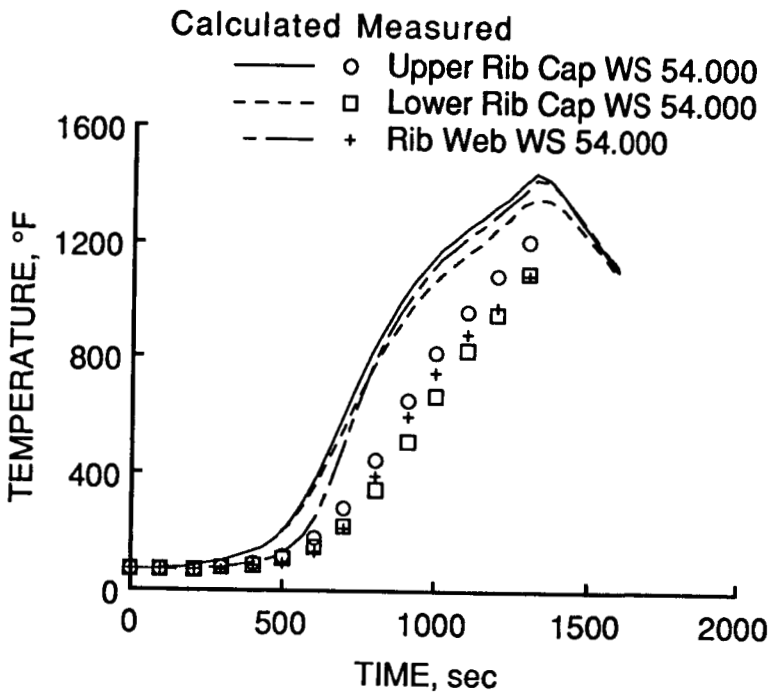

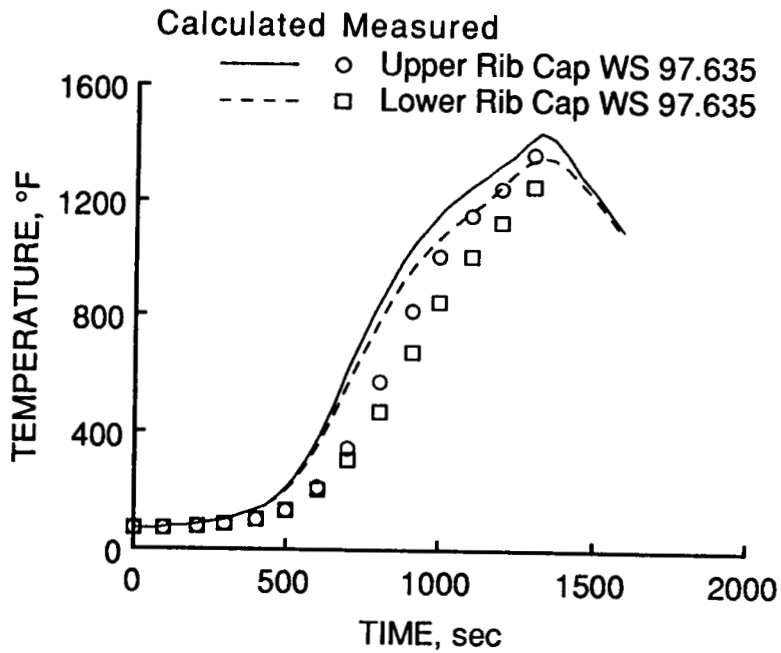

Comparison Between Measured and Calculated Structural Panel Temperature Distributions (Figure 17)

Figure 17 is a comparison between measured and calculated temperature distributions on the lower structural panel of the inboard center bay at t = 800 seconds. The dome–shaped temperature distribution implies the effect of the spar and rib caps act as heat sinks. The center structural panel calculated temperatures are in good agreement with measured data. However, the measured temperature gradients are steeper near the structural panel edges than the calculated gradients. This suggest that the thermal mass of the spar and rib caps may be to small or more likely a heat loss into the adjacent transition and support structure assemblies. Note that these plots are constructed using a distance weighted least squares smoothing algorithm and the measured temperature distributions may be distorted somewhat because the lack of data.

Comparison Between Measured and Calculated Structural Panel Temperature Distributions

Time = 800 seconds

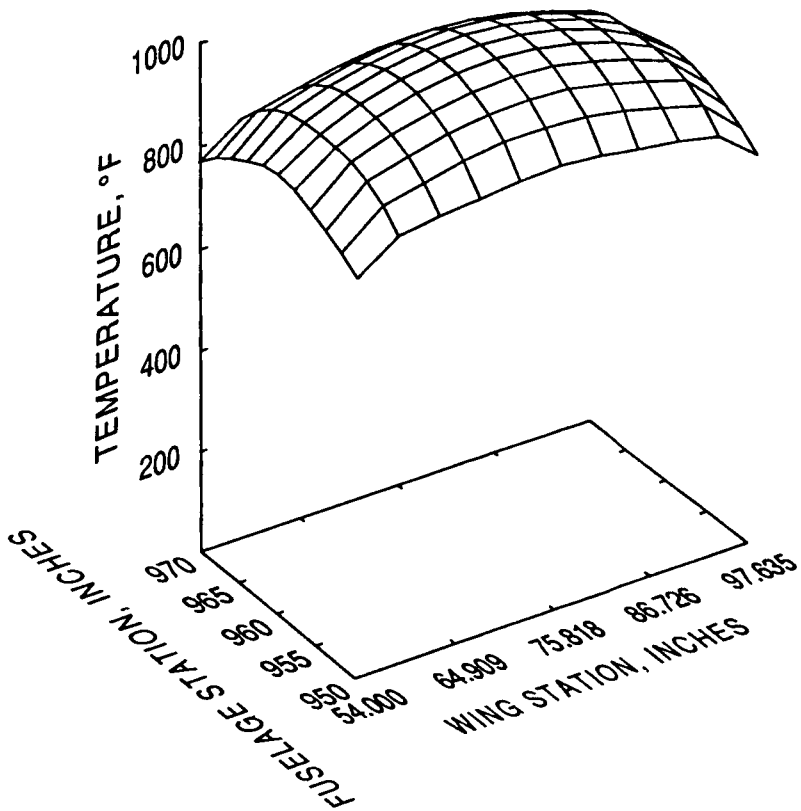

Calculated

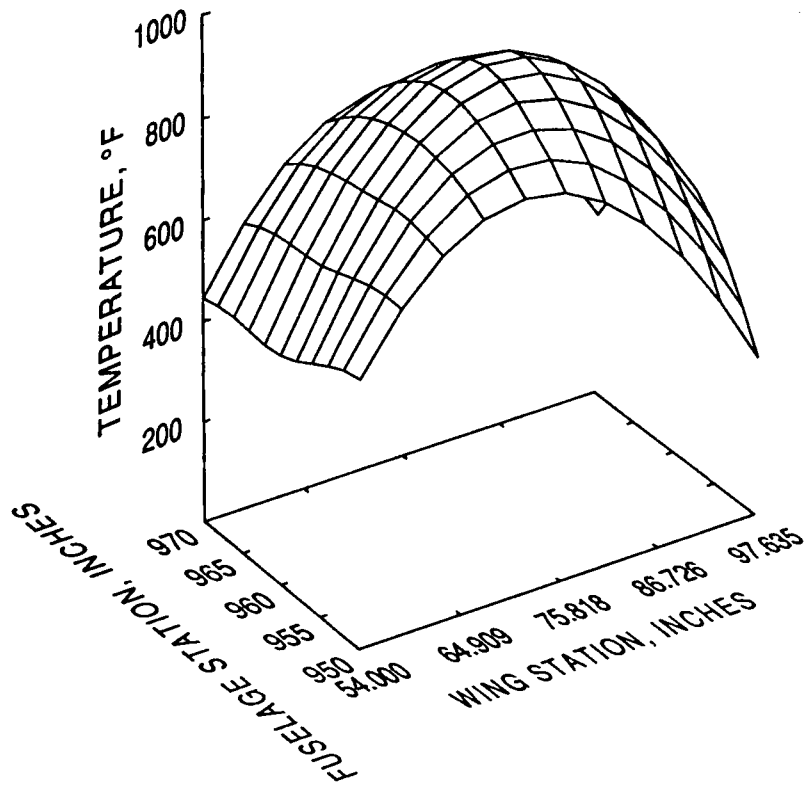

Measured

Comparison Between Measured and Calculated Structural Panel Temperature Distributions (Figure 18)

Figure 18 is a comparison between measured and calculated temperature distributions on the lower structural panel of the inboard center bay at t = 1 200 seconds. The center structural panel calculated temperatures are in good agreement with measured data. The measured temperature gradients have lessened somewhat near the structural panel edges, but the calculated temperatures show almost no gradients, having essentially reached its radiation equilibrium temperature.

Comparison Between Measured and Calculated Structural Panel Temperature Distributions

Time = 1200 seconds

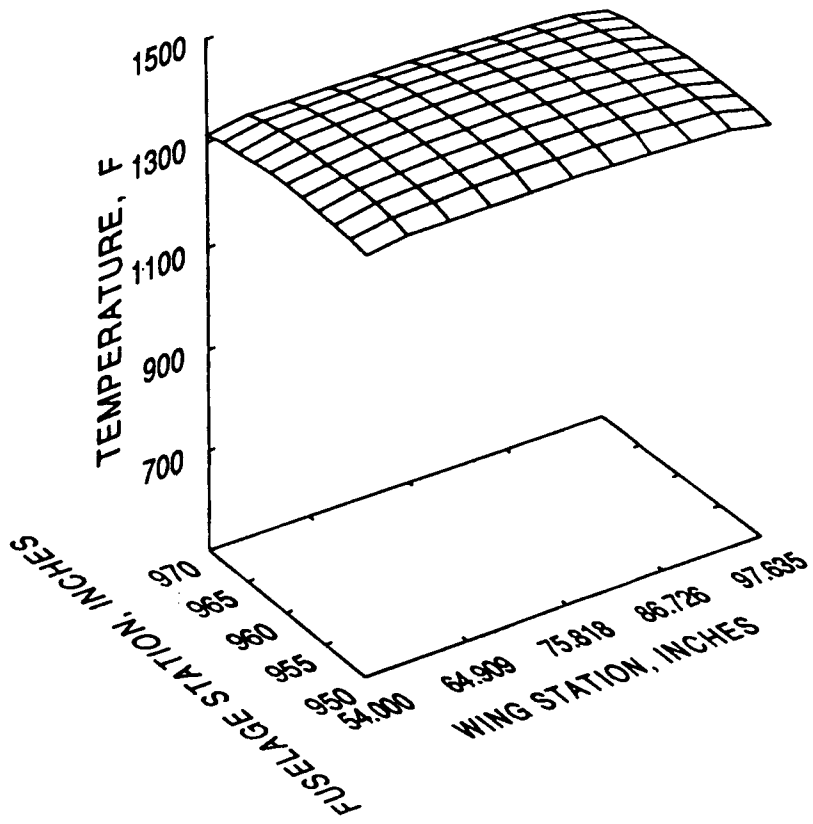

Calculated

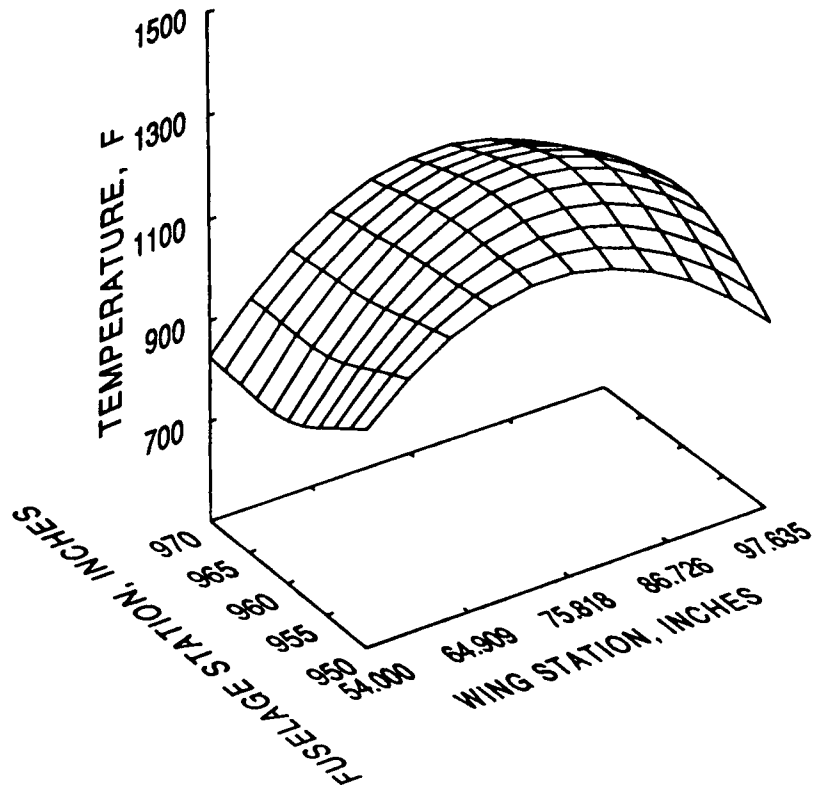

Measured

Spar Web Temperature Response with and without Internal Radiation
(Figure 19)

Figure 19 illustrates the degree to which the HWTS is dominated by radiation. The solid line represents the spar web temperature response predicted by the three dimensional SPAR thermal model with internal radiation. The dotted line represents the spar web temperature response predicted by the three dimensional SPAR thermal model without internal radiation.

Spar Web Temperature Response with and without Internal Radiation

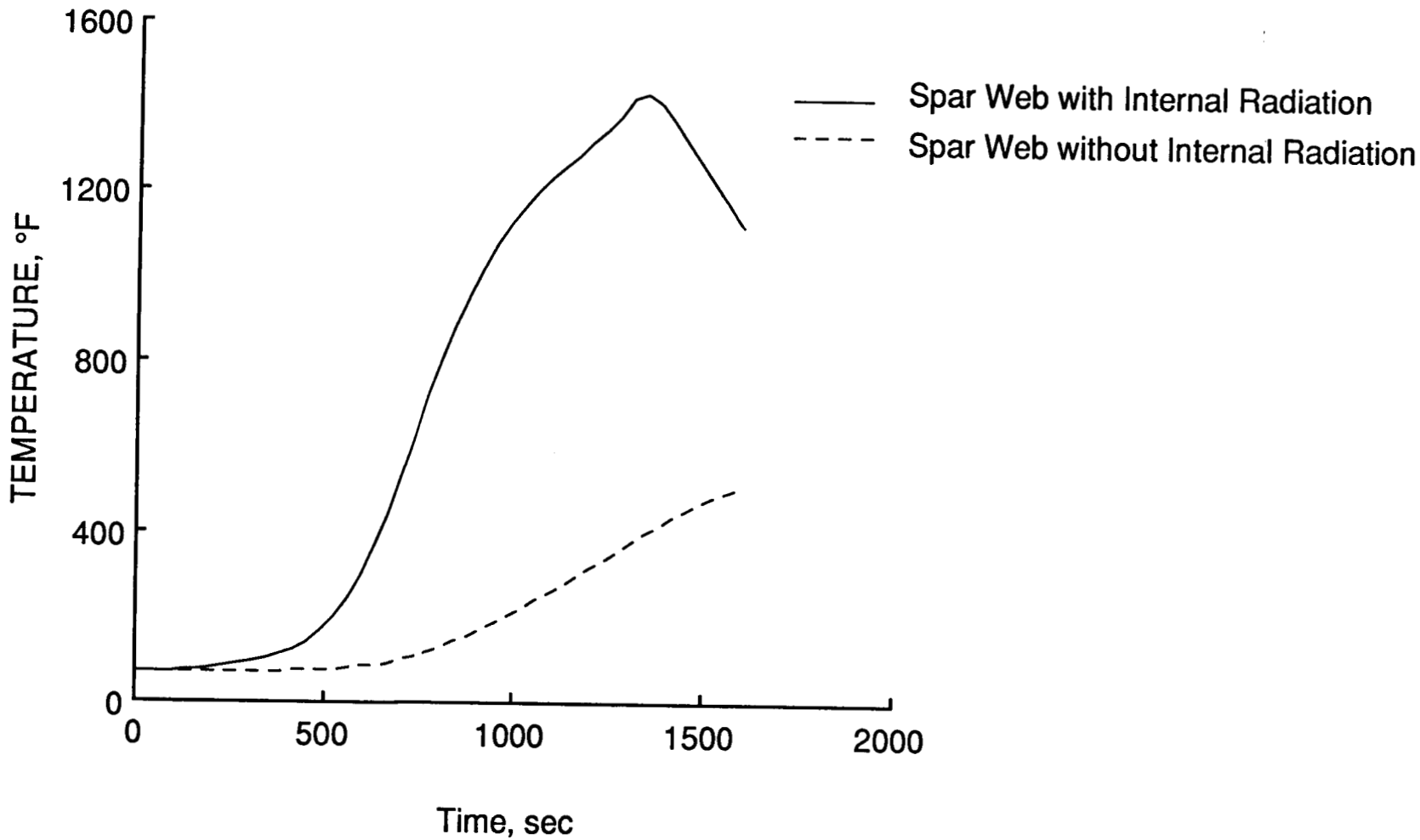

Correlation Thermal Models with Measured Data
(Figure 20)

Figure 20 shows the correlation of design, NASA, and Swanson calculated temperatures with measured temperatures for t = 600 seconds and t = 800 seconds. The solid line represents the line of perfect agreement. The dotted lines represent 50 °F reference bands above and below the line of perfect agreement. Those points falling above the line of perfect agreement overpredict the measured data and those points falling below the line of perfect agreement underpredict the measured data. For both times, clearly the design calculations overpredict the measured data. With the exception of the rib caps, the calculated data from NASA and Swanson correlate good with measured data at t = 600 seconds. At t = 800 seconds, the agreement is only fair between measured and calculated temperatures. Note that the NASA calculated temperatures at t = 800 seconds are in better agreement with measured temperatures than those calculated by Swanson. The models constructed by Swanson have a corresponding courser mesh than NASA's models but are three dimensional. This result suggest that a finer element density than Swanson used is necessary for accurate predictions of transient temperatures .

Correlation of Thermal Models with Measured Data

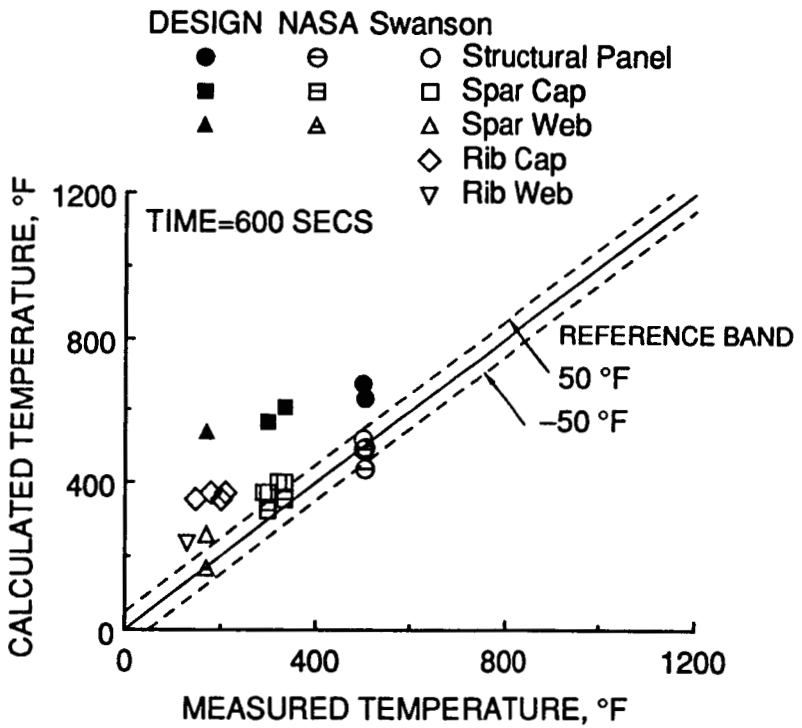

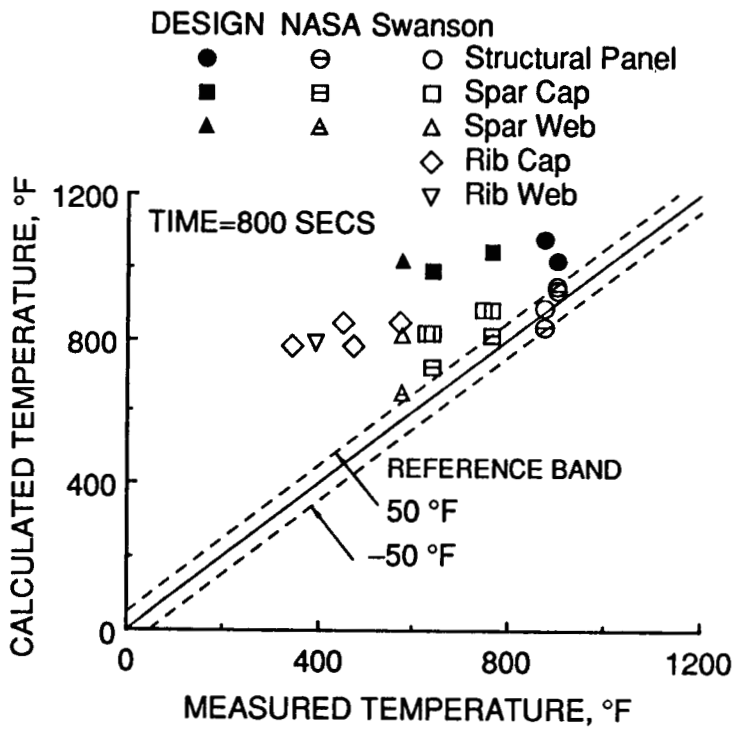

Correlation of Thermal Models with Measured Data
(Figure 21)

Figure 21 shows the correlation of design, NASA, and Swanson calculated temperatures with measured temperatures for t=1 000 seconds and t = 1 200 seconds. With the exception of the rib caps and webs, the calculated data from design, NASA and Swanson correlate good with measured data at t=1 000 seconds and t = 1 200 seconds. These results suggest that the course models used in the design are adequate for the calculation of radiaton equilibrium temperatures but inadequate for the accurate calculation of transient temperatures.

Correlation of Thermal Models with Measured Data

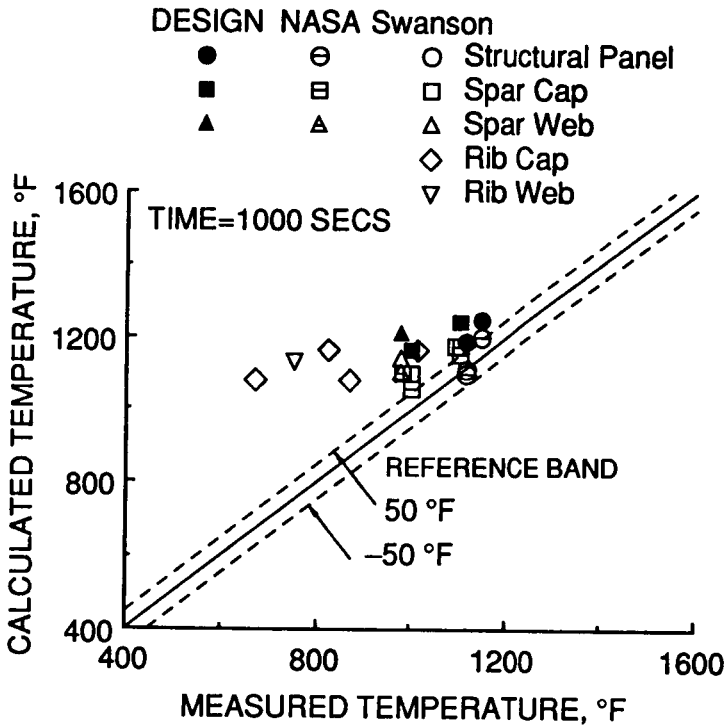

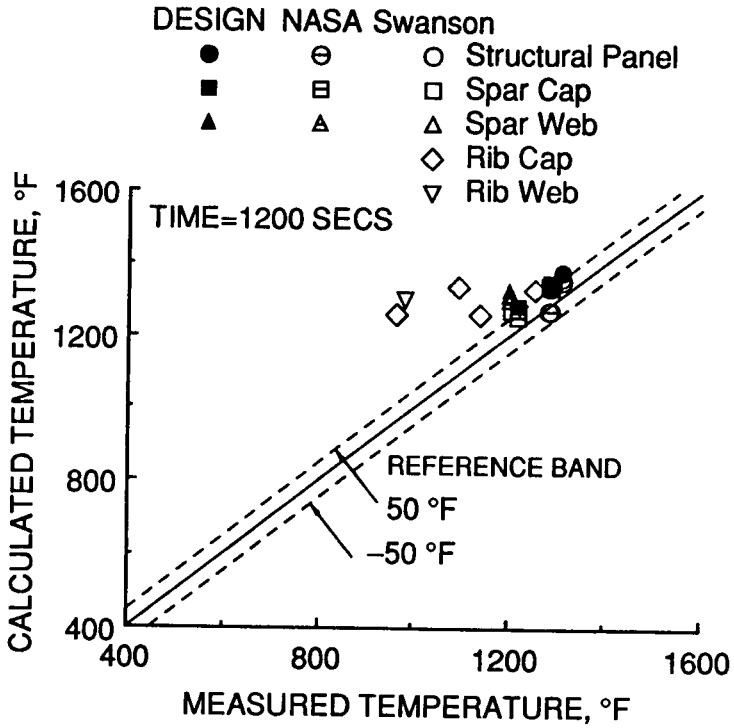

Direction Radiation Property of a Oxidized Nickel–Based Superalloy
(Figure 22)

Several factors may contribute to the higher calculated temperatures other than a heat loss from the system. The oxide coating on a metal tends to create a thin film of metal oxide dielectric or semiconductor, which tends to increase the emittance at large angles from the surface normal.

Directional Radiation Property of a Oxidized Nickel–Based Superalloy

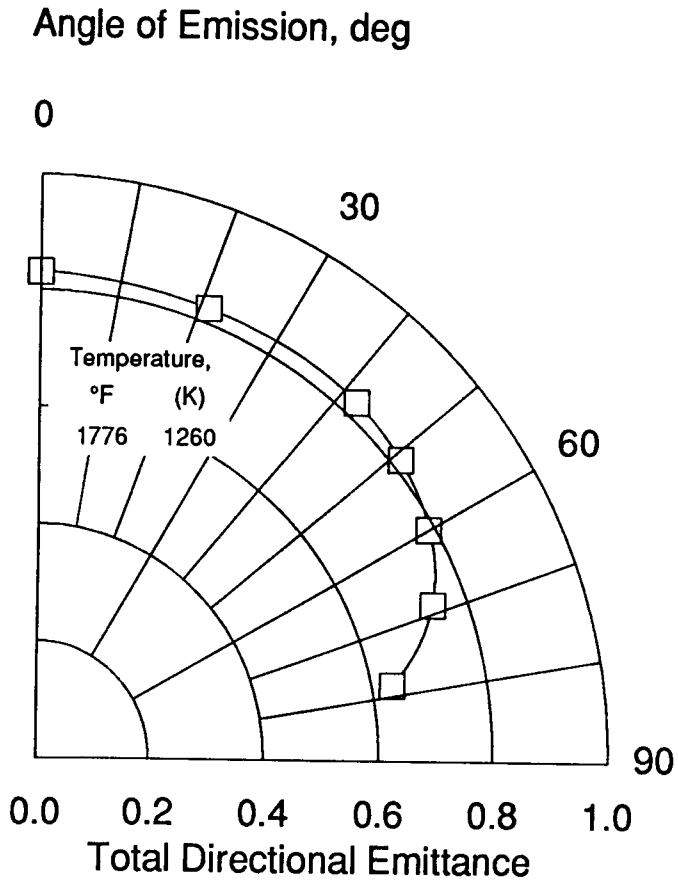

Effect of Directional Radiation Properties on Web Temperatures (Figure 23)

Figure 23 illustrates how directional radiation properties effect the web temperatures A corrugated structural panel with diffuse radiating surfaces will tend to exchange energy uniformly with the rib and spar webs. A corrugated structural panel with directional radiating surfaces will tend exchange a greater percentage of energy to the spar webs than the rib webs. Consequently, calculated temperature histories assuming diffuse radiating surfaces will tend to overpredict rib temperatures.

Effect of Directional Radiation Properties on Web Temperatures

Diffuse Radiating Surfaces

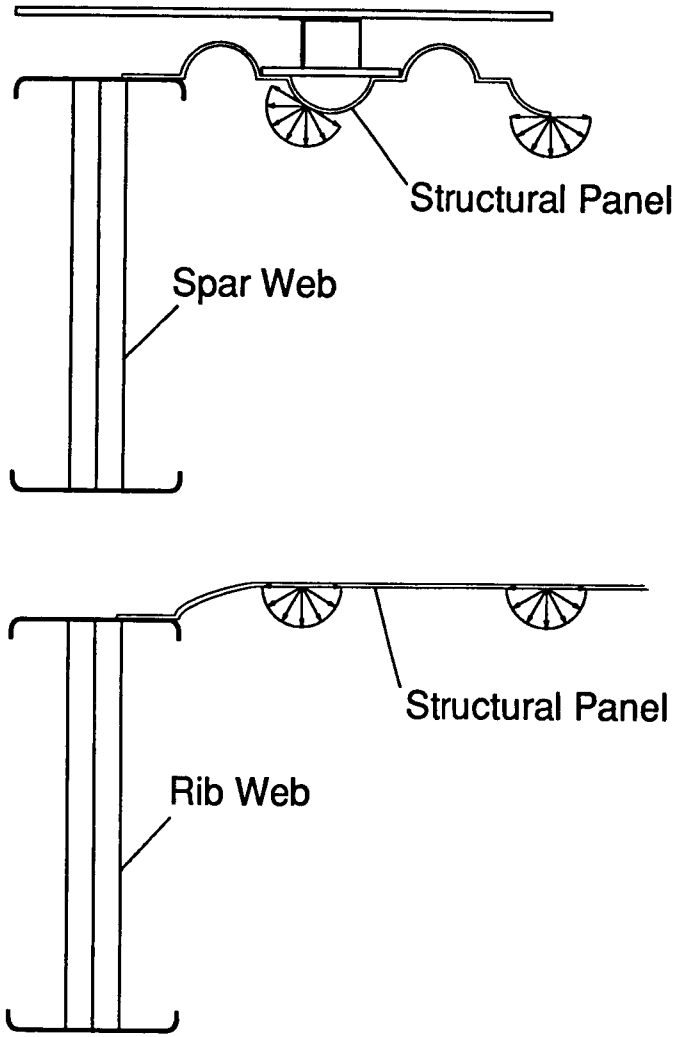

Directional Radiating Surfaces

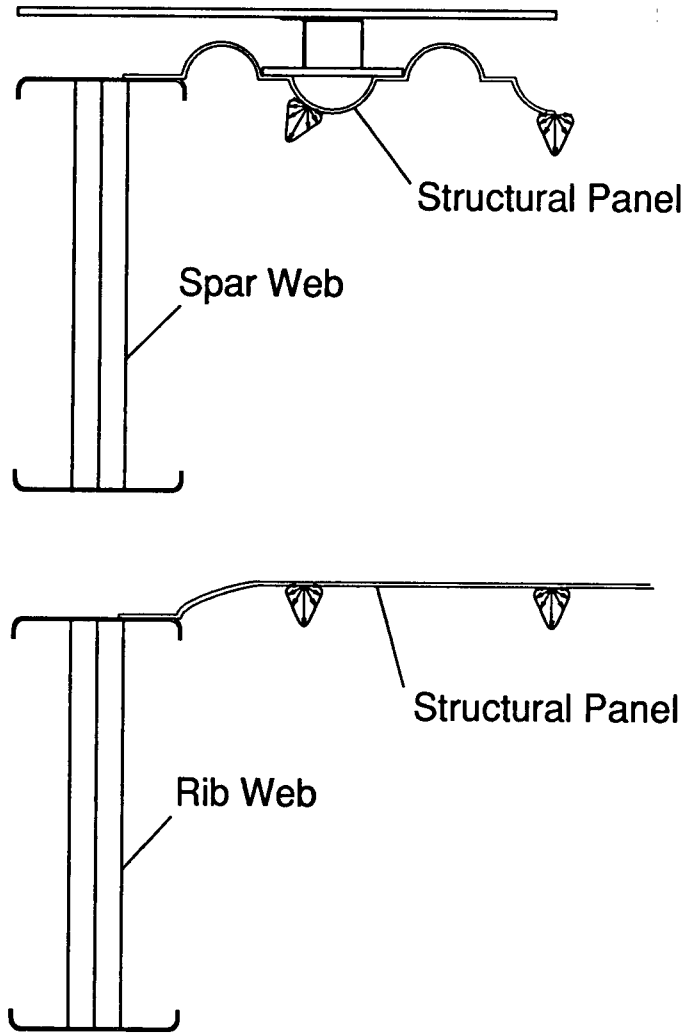

Conclusions

- The dominant mechanism of heat transfer in the HWTS is radiation and conduction heat transfer in these thin gauge type structures is at least an order of magnitude smaller than radiation heat transfer

- Comparisons between measured and calculated data suggest that finer nodalizations are required

- Measured data suggest that a spanwise heat flow exists from the hotter leading edge areas to the cooler inboard areas

- In order to investigate the use of a more sophisticated radiation heat transfer model, radiometer measurements of the radiation intensity distribution throughout a typical wing box should be made

References

1. Heldenfels, R. R.: Historical Perspectives on Thermostructural Research at the NACA Langley Aeronautical Laboratory from 1948 to 1958. NASA TM–83266, 1982.

2. Heldenfels, R. R.: Structural Prospects for Hypersonic Air Vehicles. Aircraft Eng., Nov. 1966, pp. 18–20.

3. Anderson, R. A.; and Swann, R. T.: Structures for Reentry Heating. NASA TM X–313, 1960.

4. Pride, R. A.; Royster, D. M.; and Helms, B. F.: Experimental Study of a Hot Structure for a Reentry Vehicle. NASA TM X–314, 1960.

5. Plank, P. P.; Sakata, I. F.; Davis, G. W.; and Richie, C. C.: Hypersonic Cruise Vehicle Wing Structure Evaluation. NASA CR–1568, 1970.

6. Plank, P. P.; Sakata, I. F.; Davis, G. W.; and Richie, C. C.: Substantiation Data for Hypersonic Cruise Vehicle Wing Structure Evaluation. NASA CR–66897–1, –2, –3, 1970.

7. Fields, R. A.: Dryden Flight Research Center Hot Structures Research. Recent Advances in Structures for Hypersonic Flight. NASA CP–2065, 1978, pp. 707–756.

8. Plank, P. P.; and Penning, F. A.: Hypersonic Wing Test Structure Design, Analysis, and Fabrication. NASA CR–127490, 1973.

9. Siegel, W. H.: Experimental and Finite Element Investigation of the Buckling Characteristics of a Beaded Skin Panel for a Hypersonic Aircraft. NASA CR–144863, 1978.

10. Fields, R. A.; Reardon, L. F.; and Siegel, W. H.: Loading Tests of a Wing Structure for a Hypersonic Aircraft. NASA TP–1596, 1980.

11. Dixon, S. C.: NASA R&T for Aerospace Plane Vehicles—Progress and Plans. NASA TM–86429, 1985.

12. Quinn, R. D.; and Fields, R. A.: Comparison of Measured and Calculated Temperatures for a Mach 8 Hypersonic Wing Test Structure. NASA TM–85918, 1986.

13. Plank, P. P.; and Penning, F. A.: Hypersonic Wing Test Structure, Preliminary Draft of a Portion of the Final Report, Part I—Design, Task 2—Wing Temperatures. Martin Marietta Corporation, MCR–72–96, Issue 2, Denver, Colorado, December 1972.